International Journal of Automotive Technology, Vol. 22, No. 6, pp. 1557–1567 (2021)
DOI 10.1007/s12239–021–00134–z

pISSN 1229–9138/ eISSN 1976–3832

PATH PLANNING FOR VEHICLE ACTIVE COLLISION AVOIDANCE BASED ON VIRTUAL FLOW FIELD

Jian Liu[1)], Jie Ji[1)*], Yue Ren[1)], Yanjun Huang[2)] and Hong Wang[3)]

[1)]College of Engineering and Technology, Southwest University, Chongqing 400715, China
[2)]School of Automotive Studies, Tongji University, Shanghai 201804, China
[3)]School of Vehicle and Mobility, Tsinghua University, Beijing 100091, China

(*Received 23 October 2020; Revised 4 March 2021; Accepted 20 March 2021*)

ABSTRACT–According to the inherent nature of the fluid that can naturally avoid obstacles, a path planning method for active collision avoidance of autonomous vehicles is presented based on the virtual flow field. Firstly, the mathematical model of the virtual flow field on the road is established by using the theory of hydrodynamics. Then a fifth degree polynomial curve is adopted to construct the virtual hazard area of the obstacle vehicle to prevent the fluid into this area, and it can be easily resized by adjusting the parameters of the lateral and longitudinal safety distance. Finally, Computational Fluid Dynamics (CFD) simulations are performed to quantitative predict the dynamic behavior of the ego vehicle on the straight or curved road and the desired path for active collision avoidance can be determined based on the calculation result of the flow field. The simulation results show that the proposed path planning method takes into account the dynamic characteristics and kinematic constraints of the vehicle, and ensures that the vehicle doesn't collide with the dynamic and static obstacles on the road.

KEY WORDS : Virtual flow field, Collision avoidance, Computational fluid dynamics, Path planning, Autonomous vehicle

NOMENCLATURE

V	: velocity vector of the fluid, m/s
ρ	: density, kg/m^3
F_b	: body force acting on the fluid element, N
F_s	: surface force acting on the fluid element, N
f_x	: the component of body force in the *x*-direction, N
f_y	: the component of body force in the *y*-direction, N
σ_{xx}	: normal stress, N/m^2
τ_{yx}	: shear stress, N/m^2
a	: acceleration, m/s^2
μ	: dynamic viscosity, kg/(m·s)
d	: safety distance in the lateral direction, m
s	: safety distance in the longitudinal direction, m
R	: turning radius of the vehicle, m
C_f	: cornering stiffness of the front tire, N/rad
C_r	: cornering stiffness of the rear tire, N/rad
l_f	: distance from the CG to the front axle, m
l_r	: distance from the CG to the rear axle, m
ω_r	: yaw rate of the vehicle, rad/s
I_z	: yaw moment of inertia, kg·m^2
δ_f	: steering angle of front wheel, rad

*Corresponding author. e-mail: jijiess@swu.edu.cn

1. INTRODUCTION

The active collision avoidance system of autonomous vehicles can effectively prevent the occurrence of traffic accidents and significantly improve the safety of the vehicle (Rasekhipour *et al.*, 2017). Therefore, related intelligent technologies have been extensively studied in recent years, which can be summarized into the following four subsystems: perception (Asvadi *et al.*, 2018; Andrade *et al.*, 2019; Caltagirone *et al.*, 2019), decision-making (Gindele *et al.*, 2015; Li *et al.*, 2018), path planning (Dolgov *et al.*, 2010; Chu *et al.*, 2015; Hu *et al.*, 2018), and path tracking (Park *et al.*, 2015; Xia *et al.*, 2016; Brown *et al.*, 2017). Path planning is one of the basic operations required to realize collision avoidance for autonomous driving vehicles. With information about obstacles location given by onboard sensors and road geometry information provided by highly automated driving map, a path planner generates a dynamic path for the vehicle to avoid collision with other vehicles or obstacles (Paden *et al.*, 2016). Path planning has been widely studied by scholars for decades, and many methods have been developed for autonomous vehicles. Graph search based algorithms, such as Dijkstra (1959) and A* algorithm (Hart *et al.*, 1968), are used to find the shortest path in the state space. The autonomous vehicle "junior" from Stanford University used a modified version of the A* (hybrid A*) to plan a kinematically feasible trajectory in a discrete four-dimensional

grid that contains the *x*-*y* position of the vehicle center, the heading direction, and the direction of motion, either forward or reverse (Montemerlo *et al.*, 2008). The artificial potential field (APF) method is usually to generate a virtual potential field of obstacles and the target, and then the path in the steepest descent direction of the potential field is regarded as the reference path of the vehicle (Khatib, 1986). Ji *et al.* (2017) constructed a three-dimensional potential field through the trigonometric function of the road and the exponential function of the obstacle to generate a collision-free path for the vehicle. Another type of method is to directly use geometric curves as the local trajectory for vehicle collision avoidance, such as polynomial curves (Glaser *et al.*, 2010), Bezier curves (Han *et al.*, 2010), and spline curves (Berglund *et al.*, 2009). However, because geometric curves generally have specific functional expressions, which are not convenient to adjust the path flexibly in the dynamic traffic environment (Chen *et al.*, 2019).

In recent years, the phenomenon that water can automatically avoid rocks in the river has attracted the attention of scholars (Yao *et al.*, 2016). Inspired by this natural phenomenon, a path planning method based on the fluid flow has been proposed in the latest studies. The advantage of this method is that the planned path is extremely smooth and does not fall into a local minimum because the fluid can always find an exit in the environment. Song *et al.* (2018) constructed flow fields according to a variety of traffic scenarios and set up inlets and outlets for the fluid at appropriate locations. Then the flow field is numerically calculated to obtain the reference path topology and the steering reference angle of the vehicle. However, when the fluid velocity is fast, the turbulence or recirculation will occur in the flow field, so it only focuses on the low-speed maneuvering. Cheng *et al.* (2020) proposed a virtual fluid flow model of the viscous fluid between two parallel plates or around a cylinder, and the integrated functions of lane-keeping and collision avoidance of the vehicle can be realized based on this model. But the various constraints of the vehicle are not considered in this paper and the simulation scenario considers only a few common traffic conditions. Path planning methods for unmanned aerial vehicles (UAV) based on fluid flow have also been studied (Wang *et al.*, 2015). But the complex traffic environment and constraints of vehicles are completely different from UAV, it is difficult to use these methods directly for autonomous vehicles. Overall, the application of fluid flow to solve the problem of path planning in collision avoidance is still in the preliminary stage, which needs to be studied in detail in the future work.

In this paper, a path planning method for vehicle active collision avoidance is proposed. Firstly, the virtual flow field of the road is constructed based on the theory of hydrodynamics (Anderson and Wendt, 1995; Kong, 2014). The virtual fluid is supposed to be incompressible, so it can definitely flow out from the expected outlet in the flow field, which ensures that a feasible path can be generated in any scenario. Then considering the relationship between the velocity of the ego vehicle and the obstacle, a hazard area of the obstacle based on the fifth degree polynomial curve is constructed to prevent the inflow of fluid. At last, the numerical method of CFD is utilized to calculate the flow field and the collision-free path can be obtained. In addition, simulation scenarios are extended to curve road and moving obstacle scenarios. The simulation results verify the effectiveness of the proposed method.

2. VIRTUAL FLOW FIELD MODEL OF THE ROAD

The establishment of an accurate and reliable virtual fluid field model of the road is a necessary foundation for obtaining a desired path for collision avoidance. An example of the virtual flow field considering an obstacle on a straight road is shown in Figure 1. The entire surface of the road is treated as a flow field and the fluid is set to flow in from the inlet on the left side of the road and flow out from the outlet on the right side. The remaining boundaries of the flow field are set as static and non-slip walls. It can be observed that the flowing fluid will automatically avoid the obstacle at the bottom of the flow field.

In Figure 1, the streamlines represent the flow field of the fluid. A Cartesian coordinate system of the flow field is set up, where the *x*-direction is the longitudinal direction of the road and the *y*-direction is perpendicular to the *x*-direction and points to the left side. Then the flow parameters of each point in the flow field are related to the location and time. For example, the velocity vector of the fluid in the flow field can be expressed as:

$$\boldsymbol{V}: (x, y, t) \rightarrow \begin{pmatrix} u = u(x, y, t) \\ v = v(x, y, t)) \end{pmatrix} \tag{1}$$

An infinitesimal quadrilateral fluid element *ds* at any position of the flow field is taken out for analysis, as shown in Figure 1. Its side lengths are *dx* and *dy* respectively, and its sides are parallel to the coordinate axis. The fluid element must meet the following two conditions:

a) It is infinitesimal macroscopically, which is the same as the definition in calculus;

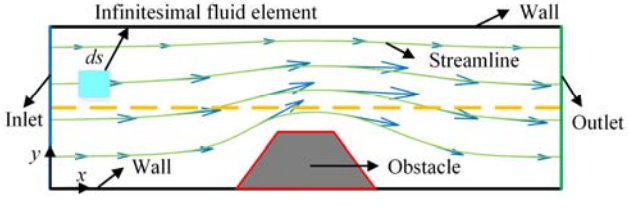

Figure 1. Virtual flow field of the road.

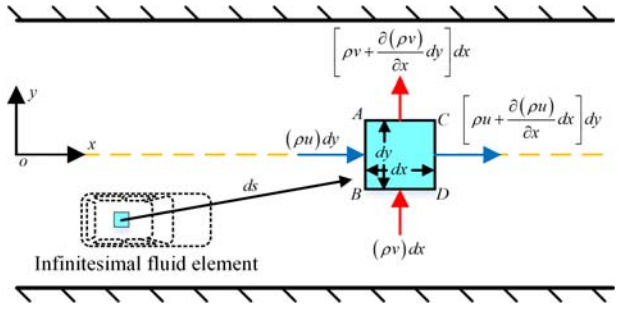

Figure 2. Mass flow of the fluid element.

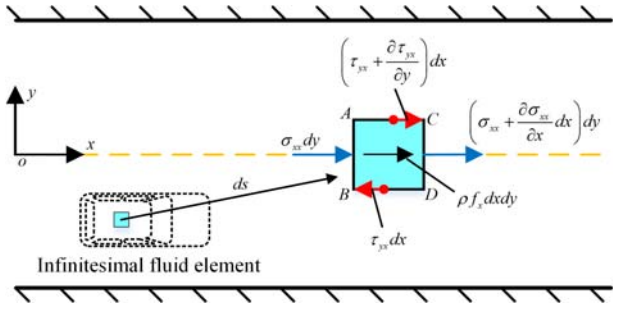

Figure 3. Force of the fluid element in the x direction.

b) It is also large enough microscopically and contains enough fluid molecules so that it can be regarded as a continuous medium.

Since the movement of the fluid follows the basic laws of physics, we establish a mathematical model of the virtual flow field of the road based on the theory of hydrodynamics. The mass flow on each side of the infinitesimal fluid element is shown in Figure 2.

In the x-direction, the mass of the net inflow can be expressed as:

$$(\rho u)dy-\left[\rho u+\frac{\partial(\rho u)}{\partial x}dx\right]dy=-\frac{\partial(\rho u)}{\partial x}dxdy \tag{2}$$

where ρ is the density of the virtual fluid.

In the y-direction, the mass of the net inflow can be expressed as:

$$(\rho v)dx-\left[\rho v+\frac{\partial(\rho v)}{\partial y}dy\right]dx=-\frac{\partial(\rho v)}{\partial y}dxdy \tag{3}$$

The original mass of the fluid element is $\rho dxdy$, and the mass increment of the fluid element per unit time is $\frac{\partial\rho}{\partial t}dxdy$. According to the conservation of mass, the differential form of the continuity equation can be deduced as:

$$\frac{\partial\rho}{\partial t}+\frac{\partial(\rho u)}{\partial x}+\frac{\partial(\rho v)}{\partial y}=0 \tag{4}$$

Then we consider the relationship between the movement and the force of the fluid element. In the virtual flow field of the road, the force acting on the fluid element includes the following two parts:

a) Body force, which acts on the entire fluid element by certain force fields, such as gravity;
b) Surface force, which acts on the surface of the fluid element and contains normal stress and shear stress.

Figure 3 shows the force acting on the fluid element in the x-direction, where f_x represents the component of the body force in the x-direction. σ_{xx} denotes the normal stress, and τ_{yx} indicates the shear stress.

In the x-direction, the body force F_b acting on the fluid element can be expressed as:

$$F_b=\rho f_x dxdy \tag{5}$$

In the x-direction, the surface force F_s acting on the fluid element can be expressed as:

$$\begin{aligned}F_s&=\left[\left(\sigma_{xx}+\frac{\partial\sigma_{xx}}{\partial x}dx\right)-\sigma_{xx}\right]dy\\&+\left[\left(\tau_{yx}+\frac{\partial\tau_{yx}}{\partial y}dy\right)-\tau_{yx}\right]dx\\&=\left(\frac{\partial\sigma_{xx}}{\partial x}+\frac{\partial\tau_{yx}}{\partial y}\right)dxdy\end{aligned} \tag{6}$$

The acceleration of the moving fluid element is determined by the material derivative, and the expression for the acceleration of the fluid element in the x-direction can be written as:

$$a_x=\frac{du}{dt}=\frac{\partial u}{\partial t}+u\frac{\partial u}{\partial x}+v\frac{\partial u}{\partial y} \tag{7}$$

Combining Equations (5), (6) and (7), according to Newton's second law, the differential equation of motion in the x-direction can be deduced as:

$$\frac{\partial u}{\partial t}+u\frac{\partial u}{\partial x}+v\frac{\partial u}{\partial y}=f_x+\frac{1}{\rho}\left(\frac{\partial\sigma_{xx}}{\partial x}+\frac{\partial\tau_{yx}}{\partial y}\right) \tag{8}$$

For the Newtonian fluid, the shear stress is proportional to

the velocity gradient, which can be expressed as:

$$\tau = \mu \frac{du}{dy} \tag{9}$$

where μ represents the dynamic viscosity of the virtual fluid.

The shear stress and normal stress of Newtonian fluid can be presented as:

$$\begin{cases} \tau_{yx} = \mu\left(\dfrac{\partial u}{\partial y} + \dfrac{\partial v}{\partial x}\right) \\ \sigma_{xx} = -p + 2\mu \dfrac{\partial u}{\partial x} \end{cases} \tag{10}$$

where p is the pressure of the virtual fluid.

Substituting Equation (10) into Equation (8), the differential equation of motion in the x-direction can be deduced as:

$$\begin{aligned} \frac{\partial u}{\partial t} + u\frac{\partial u}{\partial x} + v\frac{\partial u}{\partial y} = f_x - \frac{1}{\rho}\frac{\partial p}{\partial x} + \frac{\mu}{\rho}\left(\frac{\partial^2 u}{\partial x^2} + \frac{\partial^2 u}{\partial y^2}\right) \\ + \frac{\mu}{\rho}\frac{\partial}{\partial x}\left(\frac{\partial u}{\partial x} + \frac{\partial v}{\partial y}\right) \end{aligned} \tag{11}$$

Similarly, the differential equation of motion in the y-direction can be deduced as:

$$\begin{aligned} \frac{\partial v}{\partial t} + u\frac{\partial v}{\partial x} + v\frac{\partial v}{\partial y} = f_y - \frac{1}{\rho}\frac{\partial p}{\partial y} + \frac{\mu}{\rho}\left(\frac{\partial^2 v}{\partial x^2} + \frac{\partial^2 v}{\partial y^2}\right) \\ + \frac{\mu}{\rho}\frac{\partial}{\partial y}\left(\frac{\partial u}{\partial x} + \frac{\partial v}{\partial y}\right) \end{aligned} \tag{12}$$

To obtain a collision-free path for the autonomous vehicle under any circumstance, the mass flow rate at the inlet and outlet should be equivalent to ensure that the fluid can always find the outlet of the virtual flow field. Therefore, the fluid should be incompressible, i.e. the density ρ is constant. In addition, the external forces, such as gravity, and the heat exchange need not to be taken into account. So the differential equations of the virtual flow field of the road can be expressed as:

$$\frac{\partial u}{\partial x} + \frac{\partial v}{\partial y} = 0 \tag{13}$$

$$\begin{cases} \dfrac{\partial u}{\partial t} + u\dfrac{\partial u}{\partial x} + v\dfrac{\partial u}{\partial y} = -\dfrac{1}{\rho}\dfrac{\partial p}{\partial x} + \dfrac{\mu}{\rho}\left(\dfrac{\partial^2 u}{\partial x^2} + \dfrac{\partial^2 u}{\partial y^2}\right) \\ \dfrac{\partial v}{\partial t} + u\dfrac{\partial v}{\partial x} + v\dfrac{\partial v}{\partial y} = -\dfrac{1}{\rho}\dfrac{\partial p}{\partial y} + \dfrac{\mu}{\rho}\left(\dfrac{\partial^2 v}{\partial x^2} + \dfrac{\partial^2 v}{\partial y^2}\right) \end{cases} \tag{14}$$

In this way, the differential equation of virtual flow field is established according to the road geometry and the theory of hydrodynamics. By solving the above equations, the fluid state can be obtained and used for path planning for collision avoidance.

3. PATH PLANNING BASED ON THE NUMERICAL METHOD

In section 2, we propose a virtual flow field of the road based on hydrodynamics to plan a collision-free path for the vehicle. In order to obtain numerical results of the virtual flow field, the CFD method is adopted to solve the nonlinear partial differential equation of second order in Equation (14).

3.1. Geometric Topology of Road with Obstacle

Since obstacles on the road are important factors affecting the virtual flow field and collision-free path, a geometric model of the virtual road flow field with an obstacle needs to be established first in this section. An example of the geometric model of a straight road with an obstacle is shown in Figure 4. For the obstacle vehicle in front of the ego vehicle, a hazard area is constructed so that fluid cannot flow into this area, which is represented by the red dotted line.

To make the fluid flow steadily and avoid the vortex or reflux in the flow field, the shape of the obstacle hazard area must be relatively smooth. For polynomial curves have been successfully applied to the path planning of autonomous vehicles (Glaser *et al.*, 2010), in this study, a fifth degree polynomial curve is also used to construct the hazard area of the obstacle vehicle due to its flexibility in constructing curves:

a) The curvature is smooth, which ensures the fluid flow stably.
b) The curvature at the initial and terminal points is zero, which can be combined with the straight road well.
c) The position and shape can be easily changed by adjusting the initial and terminal points.

The curve used to construct the hazard area of obstacle can be expressed as:

$$y(x) = a_0 + a_1 x + a_2 x^2 + a_3 x^3 + a_4 x^4 + a_5 x^5 \tag{15}$$

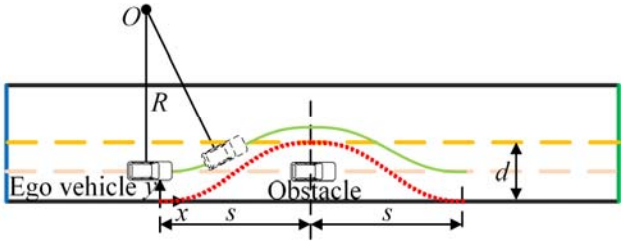

Figure 4. The diagram of the geometric model.

where y and x represent the lateral and longitudinal positions of the hazard area of the obstacle vehicle respectively. a_0, a_1, a_2, a_3, a_4 and a_5 are the coefficients to be determined.

The boundary conditions of the fifth degree polynomial curve at the initial and terminal points can be written as:

$$\begin{cases} y\big|_{x=0} = 0,\ \dot{y}\big|_{x=0} = 0,\ \ddot{y}\big|_{x=0} = 0 \\ y\big|_{x=s} = d,\ \dot{y}\big|_{x=s} = 0,\ \ddot{y}\big|_{x=s} = 0 \end{cases} \tag{16}$$

where d and s are the safety distances in the lateral and the longitudinal directions respectively, as shown in Figure 4.

According to Equations (15) and (16), the shape of the hazard area of the obstacle vehicle in the first half can be expressed as:

$$y(x) = d\left[10\left(\frac{x}{s}\right)^3 - 15\left(\frac{x}{s}\right)^4 + 6\left(\frac{x}{s}\right)^5\right] \tag{17}$$

It can be seen from Equation (17) that different lateral safety distances d and longitudinal safety distances s can be selected to reconstruct the hazard area of the obstacle vehicle according to the specific scenario.

The lateral safety distance d, which is set as 3.75 m in this study, is the width of a single lane on the structured road. For the longitudinal safety distance s, it greatly affects the length of the collision-free path. When the velocity of the ego vehicle is fast, the collision-free path should be long and smooth enough to maintain the riding stability; on the contrary, the path should be shorter and steeper to conduct the vehicle to avoid collision quickly (Chu *et al.*, 2012). So the longitudinal safety distance must be related to the velocities of the ego vehicle and the obstacle, which is defined as:

$$s_1 = \frac{v_e^{\,2} - v_o^{\,2}}{2\mu g} + d_e + d_s \tag{18}$$

where v_e and v_o are the velocities of the ego vehicle and the obstacle. μ is the adhesion coefficient of the road. g is the gravitational acceleration. d_e is the length of the ego vehicle. d_s is a headway offset (Seiler *et al.*, 1998).

To make the path obtained by the virtual flow field satisfy the kinematic and dynamic constraints of the vehicle, the radius of curvature of the fifth degree polynomial curve is taken into account to limit the minimum longitudinal safety distance of the hazard area, which can be written as:

$$r = \frac{\left(1 + \dot{y}^2\right)^{\frac{3}{2}}}{|\ddot{y}|} \tag{19}$$

Substituting Equation (17) into Equation (19), the radius of curvature of the fifth degree polynomial curves with various s can be calculated. Then the relationship between the longitudinal safety distance s and the minimum radius of curvature r_{min} is shown in Figure 5.

R is the turning radius at the center of gravity (CG) of the ego vehicle in Figure 4. The minimum turning radius when the vehicle is running on the road can be expressed as:

$$R = max\left(\frac{v^2}{a_{\max}}, \mathrm{R_m}\right) \tag{20}$$

where a_{max} is the maximum lateral acceleration, R_m is the minimum turning radius of the ego vehicle.

According to Equation (20) and Figure 5, it can be found that each R corresponds to a specific longitudinal safe distance s_2. Finally, combining with Equation (18), the longitudinal safety distance s of the hazard area of the obstacle vehicle can be deduced as:

$$s = max(s_1, s_2) \tag{21}$$

Figure 6 shows the different hazard areas of the stationary obstacle vehicle obtained by using the fifth degree polynomial curve with different velocities of the ego vehicle.

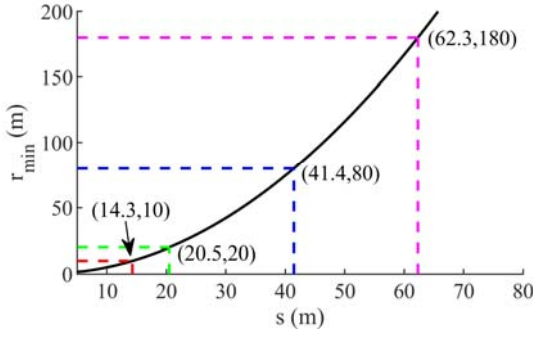

Figure 5. The relationship between the minimum radius of curvature and the longitudinal safety distance.

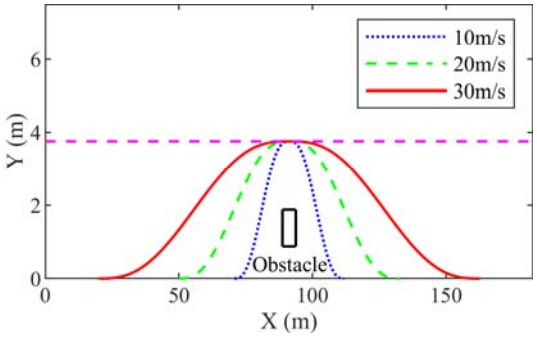

Figure 6. Hazard areas around the obstacle vehicle.

3.2. Path Generation by Using Numerical Computation

Depending on the proposed virtual flow field and the hazard area of the obstacle vehicle, the desired path for collision avoidance can be calculated numerically through computational fluid dynamics, the geometric model is discretized into triangle mesh by ANSYS Meshing, and the element size of the mesh is set as 0.3 m. Then, the laminar flow model and SIMPLE (Semi-Implicit Method for Pressure-Linked Equations) algorithm are applied to calculate the flow field by ANSYS Fluent.

Then the states of each node in the flow field can be determined after the calculation is completed. φ is used to represent the physical parameters in the flow field, which can be written as $\varphi = (x, y)$. The streamline is a smooth curve composed of different fluid particles at the same time, which is tangent to the direction of the velocity vector. The streamline can be expressed as:

$$\frac{dx}{u(x,y)} = \frac{dy}{v(x,y)} \tag{22}$$

Taking the CG of the ego vehicle at the initial position as the seed point, a streamline can be generated through numerical integration, which is regarded as the reference path for active collision avoidance of the autonomous vehicle. The streamline can also be directly displayed through the flow field visualization software CFD-Post. Moreover, the coordinates of each point on the streamline and the velocity vector field can be exported by CFD-Post, which will be further analyzed in the MATLAB.

4. SIMULATION RESULTS

In this paper, the air in the normal state is set as the virtual fluid. The density ρ is 1.225 kg/m^3 and the dynamic viscosity μ is 1.7894×10^{-5} kg/(m·s). In this section, three scenarios are set up to verify the proposed path planning method.

4.1. Vehicle Dynamics Model

To validate the feasibility of the collision-free path planned by the method based on the virtual flow field, a frequently used linearized two-degree-of-freedom vehicle model is presented as the reference model to follow the planned path, which includes the yaw and lateral motion. The state space expression of the proposed vehicle model can be written as:

$$\begin{bmatrix} \dot{v} \\ \dot{\omega}_r \end{bmatrix} = \begin{bmatrix} -\dfrac{C_f + C_r}{mu} & -\dfrac{l_f C_f - l_r C_r}{mu} - u \\ -\dfrac{l_f C_f - l_r C_r}{I_z u} & -\dfrac{l_f^2 C_f + l_r^2 C_r}{I_z u} \end{bmatrix} \begin{bmatrix} v \\ \omega_r \end{bmatrix} + \begin{bmatrix} \dfrac{C_f}{m} \\ \dfrac{l_f C_f}{I_z} \end{bmatrix} \delta_f \tag{23}$$

where v is the lateral velocity of the vehicle. ω_r is the yaw rate of the vehicle. C_f and C_r are the cornering stiffness of the front and rear tire, respectively. m is the mass of the vehicle. u is the longitudinal velocity of the vehicle. l_f and l_r are the distances from the CG of the ego vehicle to the front and rear axle, respectively. I_z is the yaw moment of inertia. δ_f is the front wheel steering angle. The main parameters of the vehicle model are shown in Table 1.

4.2. Straight Road with Stationary Obstacle

In this scenario, the ego vehicle is moving on a two-lane straight road with constant velocity (10 m/s, 20 m/s, or 30 m/s). The initial position of the ego vehicle is at the centerline of the right lane (x = 0 m, y = 1.875 m), and a stationary obstacle vehicle is in front of the ego vehicle. According to the hazard area of the obstacle vehicle in section 3, the obstacle vehicle is located at 30.28 m, 51.44 m or 81.29 m in front of the ego vehicle, respectively. Through the numerical computation of the virtual flow field, the velocity vector field and the planned path for vehicle active collision avoidance are obtained, as shown in Figure 7. The arrows indicate the velocity vector at each node. The green curve represents the collision-free path of the ego vehicle. The red curve and the right boundary enclose the hazard area of the obstacle vehicle.

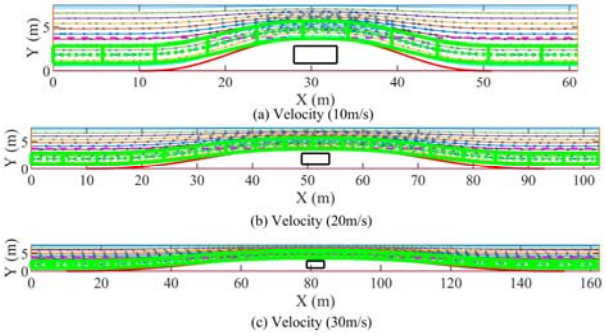

Figure 7. Planned path on the straight road with a stationary obstacle vehicle.

Table 1. The main parameters of the vehicle model.

Symbol	Value	Units
m	1270	kg
I_z	1537.6	kg·m^2
l_f	1.015	m
l_r	1.895	m
C_f	66900	N/rad
C_r	62700	N/rad

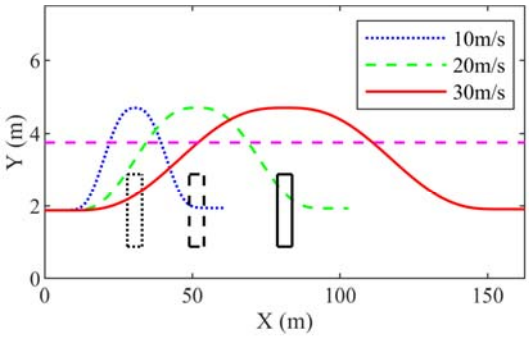

(a) Planned path

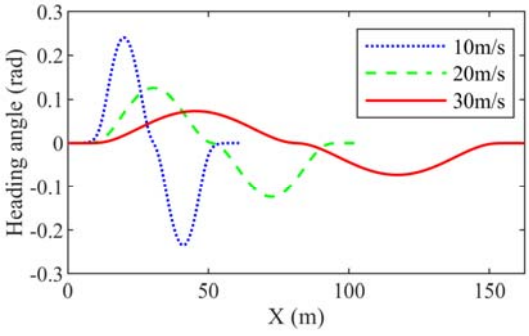

(b) Heading angle curve

Figure 8. Collision-free path and heading angle with different velocities of the ego vehicle.

As shown in Figure 7, the ego vehicle will not collide with the obstacle vehicle or road boundaries. After completing the collision avoidance, the ego vehicle returns to the original lane and continue to drive along the centerline, which indicates that the proposed approach also has the function of lane-keeping.

Figure 8 shows the comparison of the lateral position and heading angle of three collision-free paths when the velocity of the ego vehicle is different. It can be seen that the longitudinal distance of the collision-free path is longer and the path is smoother when the velocity of the ego vehicle is faster. The maximum heading angle of the three paths is also reduced from 0.24 rad at 10 m/s to 0.073 rad at 30 m/s. So the planned path designed based on the virtual flow field guides the ego vehicle to steer quickly to avoid the collision at low velocity and maintain the riding stability while avoiding collision at high velocity, which conforms to the actual situation of the vehicle collision avoidance.

Although we have set up the hazard area around the obstacle vehicle to make the ego vehicle follow the planned path successfully, it is also essential to analyze whether the planned path meets certain constraints of the vehicle. Assuming that the longitudinal velocity of the ego vehicle remains constant during the entire collision avoidance process, Figure 9 shows the comparison of the lateral acceleration of the ego vehicle obtained from the three paths in Figure 8 (a). The maximum lateral acceleration of the three paths are 3.73 m/s^2, and the change of the lateral

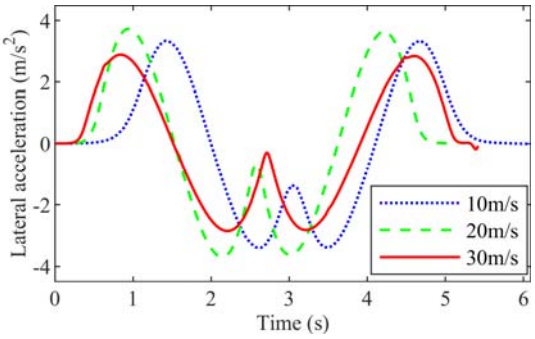

Figure 9. The comparison of the lateral acceleration.

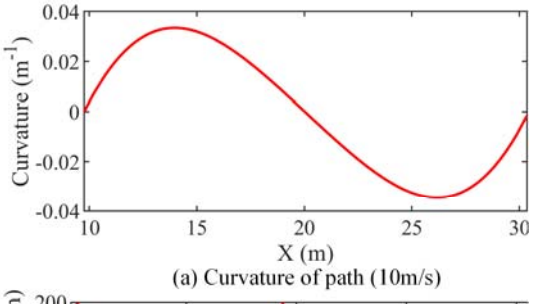

(a) Curvature of path (10m/s)

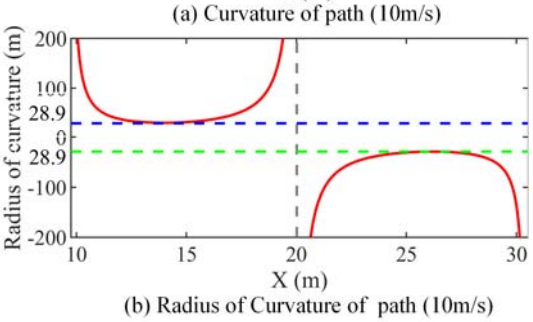

(b) Radius of Curvature of path (10m/s)

Figure 10. Simulation results of the collision-free path with velocity 10 m/s.

acceleration is relatively smooth, which satisfies the kinematic constraints of the road vehicle.

Due to the collision-free path is a relatively steep and roughly symmetric curve when the velocity of the ego vehicle is 10 m/s, only the first half of the curve needs to be analyzed. The curvature and radius of curvature of this path are shown in Figure 10. The curvature of this path changes smoothly and the minimum radius of curvature is 28.9 m, which is larger than the vehicle's minimum turning radius of 20.5 m calculated using Equation (20).

In addition, Figure 11 shows the comparison between the planned path (10 m/s) obtained from the virtual flow field and the fifth degree polynomial curve with reasonably set parameters. Compared with the fifth degree polynomial curve, the planned path by the virtual flow field method can carry out collision avoidance operation by steering in advance, and the front wheel steering angle and lateral acceleration of the vehicle is smaller.

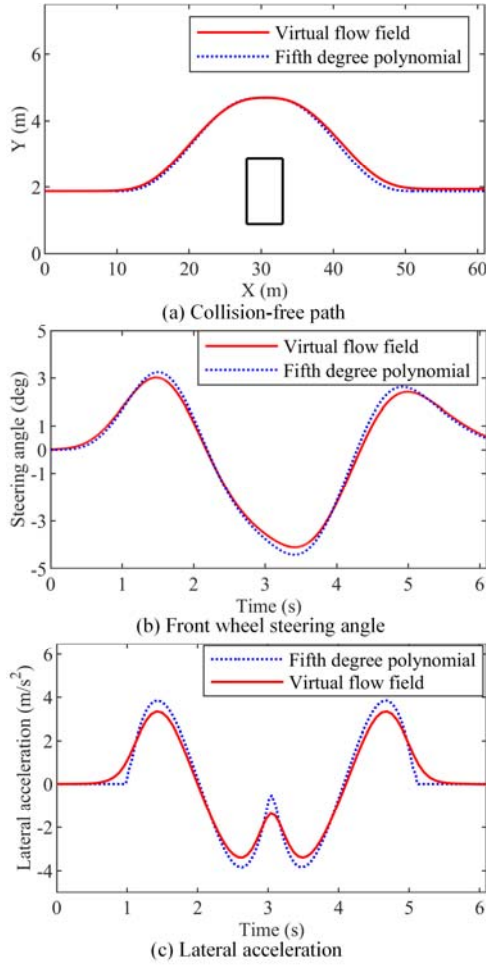

Figure 11. Comparison between the planned path (10 m/s) and the fifth degree polynomial curve.

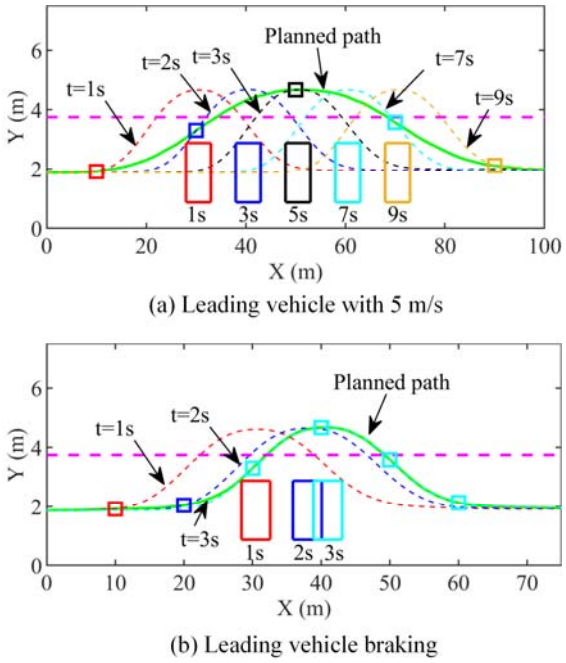

Figure 12. Planned path on the straight road with a moving obstacle vehicle.

4.3. Straight Road with Moving Obstacle

In this scenario, two vehicles are moving on a two-lane straight road with the same velocity of 10 m/s, and the leading vehicle suddenly slows or brakes at some point in the same lane. In order to ensure the safety and efficiency of the ego vehicle, a collision avoidance or overtaking path needs to be planned.

To calculate the virtual flow field numerically in the presence of moving obstacle vehicle, dynamic mesh technology of ANSYS Fluent that can control the movement of parts is applied in this paper (García *et al.*, 2015). In this case, the hazard area of the leading vehicle is set as the dynamic mesh, and the profile file is utilized to specify the motion form of the dynamic mesh. The update mode of the dynamic mesh is set to the smoothing and remeshing method. A spring smoothing model is adopted in the smoothing method to ensure the mesh quality at a slight displacement and the remeshing method utilizes a local cell reconstruction model to avoid poor mesh quality or negative volume at a large displacement. In this way, the mesh will be automatically updated in Fluent software according to the latest leading vehicle position at each time step. The other boundary conditions are kept unchanged. At last, the flow field at each time step is calculated by the numerical method in ANSYS Fluent software, and then the collision-free path can be obtained in the dynamic traffic environment.

Figure 12 shows the planned path for the ego vehicle on the straight road with moving obstacle vehicle, where the green line represents the collision-free path of the ego vehicle, the dotted curves represent the instantaneous collision avoidance path at different time steps, and the rectangles represent the leading vehicle at different time steps. In scenario (a), the leading vehicle is running at a constant velocity of 5 m/s, which is half the velocity of the ego vehicle. In scenario (b), the leading vehicle brakes suddenly and the velocity decreases from 10 m/s to zero within 2 s. In both scenarios, the planned path can guide the ego vehicle to avoid the moving obstacle. But in the dynamic environment, the length of the collision-free path in above scenarios is longer than that in the stationary obstacle scenario.

Figure 13 shows the heading angle and lateral acceleration of the collision-free path when the movement of the leading vehicle is different. In the case of the stationary obstacle in front, the maximum heading angle and lateral acceleration are 3.4 m/s^2 and 0.24 rad, respectively. In scenario (a), these two parameters are reduced to 3.13 m/s^2 and 0.22 rad, respectively. In scenario (b), these two parameters are only 0.76 m/s^2 and 0.12 rad, respectively.

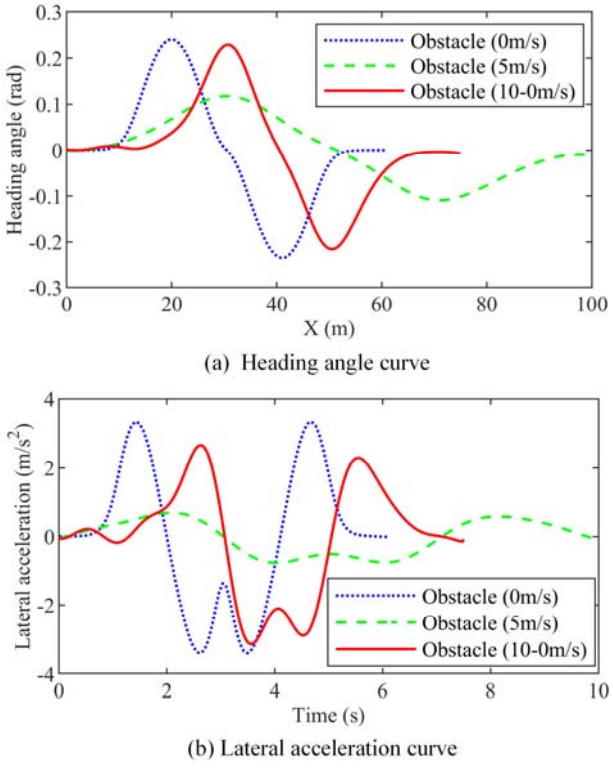

Figure 13. The heading angle and lateral acceleration of collision-free paths with various obstacles in front.

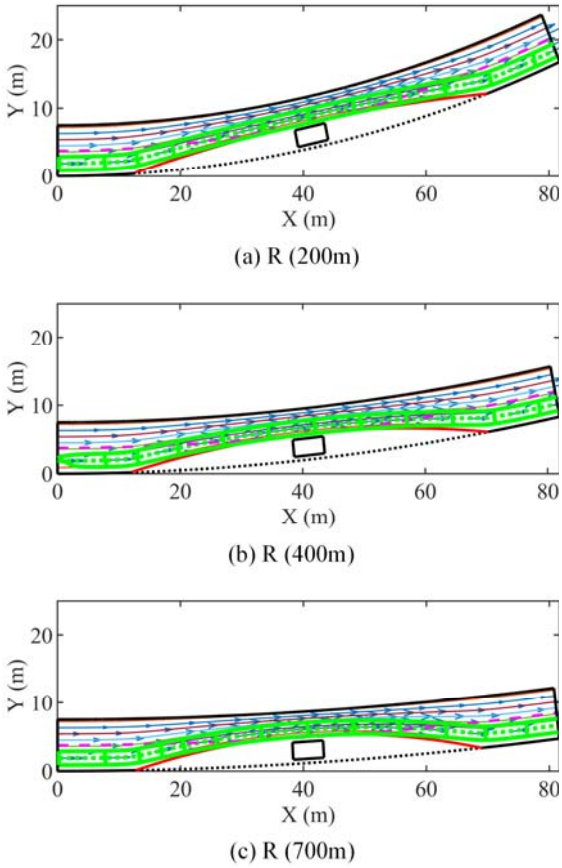

Figure 14. Planned path on the curved road with a stationary obstacle vehicle.

4.4. Curved Road with Stationary Obstacle

In this scenario, the ego vehicle is moving on a two-lane curved road with constant velocity of 10 m/s, and there is still a stationary obstacle in front of the ego vehicle. The method in the section 2 can also be used to establish the virtual flow field model of the curved road, but the fifth degree polynomial curve is not suitable for the construction of the hazard area of the obstacle vehicle on the curved road. However, the fluid has its specific inherent nature, that is, the streamline is still relatively smooth even if the shape of the hazard area of the obstacle is not absolutely smooth. Therefore, a simplified arc is utilized to replace the fifth degree polynomial curve to construct the hazard area of the obstacle vehicle on the curved road.

Figure 14 shows the planned paths when the radii of the curved road are 200 m, 400 m and 700 m respectively. The arrows indicate the velocity vector at each node in the virtual flow field. The green curve represents the collision-free path for the ego vehicle and the red curve is the hazard area of the obstacle vehicle. It can be seen that the proposed method can still plan a collision-free and smooth path for the ego vehicle on the curved road, and the ego vehicle returns to the centerline of the original lane after the collision avoidance is completed. Figure 15 shows that as the curvature of the road increases, the planned path becomes steeper.

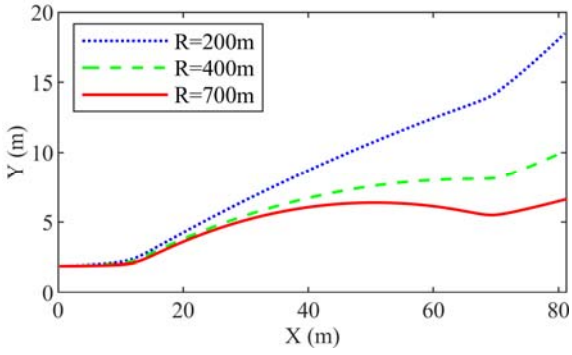

Figure 15. Collision-free paths on curved road.

The heading angle and lateral acceleration on the curved road with various radii is shown in Figure 16. Because the road is curved, the heading angle of the ego vehicle is constantly increasing, and there are obvious saltations at the beginning and end of collision avoidance. The lateral acceleration of the ego vehicle on curved roads always exists, and the maximum lateral acceleration of these three paths is 5.8 m/s^2.

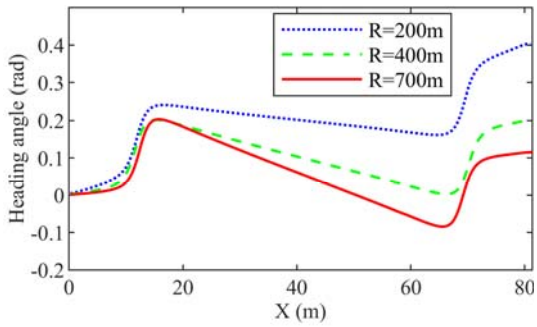

(a) Heading angle curve

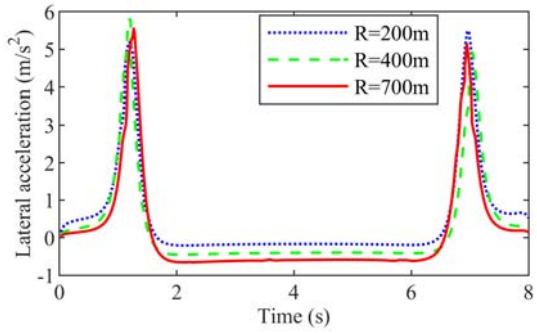

(b) Lateral accelerate curve

Figure 16. The heading angle and lateral acceleration for vehicle on the curved road with diverse radii.

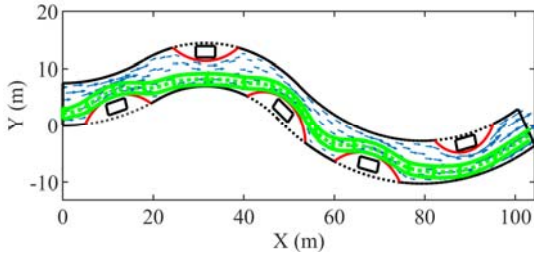

Figure 17. Planned path on the curved road with multiple obstacles.

In addition, another unique advantage of the path planning method based on the virtual flow field is the capability of path planning in the scenario with multiple obstacles. Figure 17 shows the path planned by the proposed method on the curve road with multiple obstacles, and the green curve indicates the reference path of the vehicle. The result shows that the planned path can also ensure that the vehicle will not collide with multiple obstacles and is still relatively smooth.

Based on the above simulation results, we can conclude that the path planning method based on the virtual flow field can successfully generate a particularly smooth path for the ego vehicle that satisfies the vehicle dynamics constraints. Moreover, this method has strong adaptability, which can deal with the path planning problem of vehicle active collision avoidance in a variety of scenarios such as straight road or curved road with static or moving obstacles. However, it is difficult to apply the traditional interpolation curve-based method to curved road. Finally, since the fluid has the characteristic that it can always find the outlet of the environment, which ensures that a feasible path can always be obtained even in a complex multi-obstacle environment.

5. CONCLUSION

In this paper, a path planning method based on the virtual flow field for active collision avoidance of autonomous vehicles is presented. According to the information of the road geometry and position of the obstacle, different virtual flow fields on the road are established based on the theory of hydrodynamics. Meanwhile, the presented flow field also proves that the fifth degree polynomial curve is an effective way to construct the hazard area of the obstacle vehicle, which can avoid collision by adjusting the safe distance in the lateral and longitudinal directions. In addition, the desired path for collision avoidance in various scenarios are obtained through the numerical calculation result of the flow field, and it is relatively smooth and can satisfy multiple constraints of the vehicle. After the collision avoidance is completed, the designed path can also guide the ego vehicle back to the centerline of the original lane, which indicates that the proposed approach also has the ability of lane-keeping.

In the future work, based on the virtual flow field method, the velocity planning of the ego vehicle and the path planning in more complex scenarios will be studied in more detail.

ACKNOWLEDGEMENT–This work was supported by the Fundamental Research Funds for the Central Universities [Grant No. XDJK2019B053], and Open Foundation from Chongqing Key Laboratory of Automotive Active Safety Testing Technology [Grant No. 19AKC8].

REFERENCES

Anderson, J. D. and Wendt, J. (1995). *Computational Fluid Dynamics.* McGraw-Hill. New York, USA.

Andrade, D. C., Bueno, F., Franco, F. R., Silva, R. A., Neme, J. H. Z., Margraf, E., Omoto, W. T., Farinelli, F. A., Tusset, A. M., Okida, S., Santos, M. M. D., Ventura, A., Carvalho, S. and Amaral, R. D. S. (2019). A novel strategy for road lane detection and tracking based on a vehicle's forward monocular camera. *IEEE Trans. Intelligent Transportation Systems* **20**, **4**, 1497–1507.

Asvadi, A., Garrote, L., Premebida, C., Peixoto, P. and Nunes, U. J. (2018). Multimodal vehicle detection: fusing 3D-LIDAR and color camera data. *Pattern Recognition Letters,* **115**, 20–29.

Berglund, T., Brodnik, A., Jonsson, H., Staffanson, M. and Soderkvist, I. (2009). Planning smooth and obstacle-avoiding B-spline paths for autonomous mining vehicles. *IEEE Trans. Automation Science and Engineering* **7**, **1**, 167–172.

Brown, M., Funke, J., Erlien, S. and Gerdes, J. C. (2017). Safe driving envelopes for path tracking in autonomous vehicles. *Control Engineering Practice,* **61**, 307–316.

Caltagirone, L., Bellone, M., Svensson, L. and Wahde, M. (2019). LIDAR-camera fusion for road detection using fully convolutional neural networks. *Robotics and Autonomous Systems,* **111**, 125–131.

Chen, L., Qin, D., Xu, X., Cai, Y. and Xie, J. (2019). A path and velocity planning method for lane changing collision avoidance of intelligent vehicle based on cubic 3-D Bezier curve. *Advances in Engineering Software,* **132**, 65–73.

Cheng, S., Li, L., Liu, Y. G., Li, W. B. and Guo, H. Q. (2020). Virtual fluid-flow-model-based lane-keeping integrated with collision avoidance control system design for autonomous vehicles. *IEEE Trans. Intelligent Transportation Systems*, 1–10.

Chu, K., Kim, J., Jo, K. and Sunwoo, M. (2015). Real-time path planning of autonomous vehicles for unstructured road navigation. *Int. J. Automotive Technology* **16**, **4**, 653–668.

Chu, K., Lee, M. and Sunwoo, M. (2012). Local path planning for off-road autonomous driving with avoidance of static obstacles. *IEEE Trans. Intelligent Transportation Systems* **13**, **4**, 1599–1616.

Dijkstra, E. W. (1959). A note on two problems in connexion with graphs. *Numerische Mathematik* **1**, **1**, 269–271.

Dolgov, D., Thrun, S., Montemerlo, M. and Diebel, J. (2010). Path planning for autonomous vehicles in unknown semi-structured environments. *Int. J. Robotics Research* **29**, **5**, 485–501.

García M, P., Vakkilainen, E. and Hyppänen, T. (2015). 2D dynamic mesh model for deposit shape prediction in boiler banks of recovery boilers with different tube spacing arrangements. *Fuel,* **158**, 139–151.

Gindele, T., Brechtel, S. and Dillmann, R. (2015). Learning driver behavior models from traffic observations for decision making and planning. *IEEE Intelligent Transportation Systems Magazine* **7**, **1**, 69–79.

Glaser, S., Vanholme, B., Mammar, S., Gruyer, D. and Nouvelière, L. (2010). Maneuver based trajectory planning for highly autonomous vehicles on real road with traffic and driver interaction. *IEEE Trans. Intelligent Transportation Systems* **11**, **3**, 589–606.

Han, L., Yashiro, H., Nejad, H. T. N., Do, Q. H. and Mita, S. (2010). Bezier curve based path planning for autonomous vehicle in urban environment. *IEEE Intelligent Vehicles Symp*, 1036–1042.

Hart, P. E., Nilsson, N. J. and Raphael, B. (1968). A formal basis for the heuristic determination of minimum cost paths. *IEEE Trans. Systems Science and Cybernetics* **4**, **2**, 100–107.

Hu, X., Chen, L., Tang, B., Cao, D. and He, H. (2018). Dynamic path planning for autonomous driving on various roads with avoidance of static and moving obstacles. *Mechanical Systems and Signal Processing,* **100**, 482–500.

Ji, J., Khajepour, A., Melek, W. W. and Huang, Y. (2017). Path planning and tracking for vehicle collision avoidance based on model predictive control with multiconstraints. *IEEE Trans. Vehicular Technology* **66**, **2**, 952–964.

Khatib, O. (1986). Real-time obstacle avoidance for manipulators and mobile robots. *Int. J. Robotics Research* **5**, **1**, 90–98.

Kong, L. (2014). *Engineering Fluid Mechanics.* 4th edn. China Electric Power Press. Beijing, China.

Li, L., Ota, K. and Dong, M. (2018). Humanlike driving: empirical decision-making system for autonomous vehicles. *IEEE Trans. Vehicular Technology* **67**, **8**, 6814–6823.

Montemerlo, M., Becker, J., Bhat, S., Dahlkamp, H., Dolgov, D., Ettinger, S., Haehnel, D., Hilden, T., Hoffmann, G., Huhnke, B., Johnston, D., Klumpp, S., Langer, D., Levandowski, A., Levinson, J., Marcil, J., Orenstein, D., Paefgen, J., Penny, I., Petrovskaya, A., Pflueger, M., Stanek, G., Stavens, D., Vogt, A. and Thrun, S. (2008). Junior: the stanford entry in the urban challenge. *J. Field Robotics* **25**, **9**, 569–597.

Paden, B., Cap, M., Yong, S. Z., Yershov, D. and Frazzoli, E. (2016). A survey of motion planning and control techniques for self-driving urban vehicles. *IEEE Trans. Intelligent Vehicles* **1**, **1**, 33–55.

Park, M., Lee, S. and Han, W. (2015). Development of steering control system for autonomous vehicle using geometry-based path tracking algorithm. *Etri J.* **37**, **3**, 617–625.

Rasekhipour, Y., Khajepour, A., Chen, S. and Litkouhi, B. (2017). A potential field-based model predictive path-planning controller for autonomous road vehicles. *IEEE Trans. Intelligent Transportation Systems* **18**, **5**, 1255–1267.

Seiler, P., Song, B. and Hedrick, J. K. (1998). Development of a collision avoidance system. *SAE Trans.* 1334–1340.

Song, M., Wang, N., Gordon, T. and Wang, J. (2018). Flow-field guided steering control for rigid autonomous ground vehicles in low-speed manoeuvring. *Vehicle System Dynamics* **57**, **8**, 1090–1107.

Wang, H., Lyu, W., Yao, P., Liang, X. and Liu, C. (2015). Three-dimensional path planning for unmanned aerial vehicle based on interfered fluid dynamical system. *Chinese J. Aeronautics* **28**, **1**, 229–239.

Xia, Y., Pu, F., Li, S. and Gao, Y. (2016). Lateral path tracking control of autonomous land vehicle based on ADRC and differential flatness. *IEEE Trans. Industrial Electronics* **63**, **5**, 3091–3099.

Yao, P., Wang, H. and Su, Z. (2016). Cooperative path planning with applications to target tracking and obstacle avoidance for multi-UAVs. *Aerospace Science and Technology* **54**, 10–22.